

Article

Development of an Automatic Welding System for the Boiler Tube Walls Weld Overlay

Tian Songya ^{1,†}, Adnan Saifan ^{1,2,*,†} , Gui Pengqian ¹, Imran Dawy ³ and Bassiouny Saleh ^{4,5} 

¹ College of Mechanical and Electrical Engineering, Hohai University, Changzhou 213022, China; tiansongya@126.com (T.S.); guipengqian@163.com (G.P.)

² Mechanical Engineering Dept., Faculty of Engineering, Sana'a University, Sana'a 12544, Yemen

³ School of Information Science and Engineering, East China University of Science and Technology, Shanghai 200237, China; imrandawy@mail.ecust.edu.cn

⁴ College of Mechanics and Materials, Hohai University, Nanjing 211100, China; bassiouny.saleh@alexu.edu.eg or bassiouny.saleh@hhu.edu.cn

⁵ Production Engineering Department, Alexandria University, Alexandria 21544, Egypt

* Correspondence: adnhsaifan@gmail.com; Tel.: +86-139-2104-6412 or +86-135-8434-8416

† These Authors contributed equally to this work.

Received: 9 August 2020; Accepted: 12 September 2020; Published: 15 September 2020



Abstract: Tube walls are an essential part of the thermal power plant boiler. During the operation of the boiler, the heating surface of the tube walls are exposed to furnace particles, intense heat, and chemical components resulting from the combustion reaction. These cause corrosion and wear, which permanently collapse the tubes, and affect the reliability and performance of the boiler. Therefore, a protection layer of heat and corrosion-resistant material is typically welded on the surface of the tube walls. In this study, a dedicated weld overlay automatic system is proposed. The downward welding technique with the pulse gas metal arc welding (GMAW) process is used to accomplish the proposed approach. The system generates and plans beads sequence based on the analysis of the tube walls geometry. The inverse kinematic theory was used to calculate the coordinates and transformations of the welding torch. Then, a mathematical model for the welding torch trajectory was established. A SIMOTION controller was adapted for motion control. A weld-tracking system based on the adaptive neuro-fuzzy inference system (ANFIS) was used to solve the welding distortion and the assembly error. The experiment results show that the proposed design is efficient and reliable compared to previous methods. The degree of automation and the weld overlay quality of the boiler tube walls have been notably improved.

Keywords: weld overlay; automatic welding; membrane; tube walls; weld-tracking system

1. Introduction

In recent years, researchers have been interested in studying the design of tube walls because, in the boiler, tube walls play a vital role. It has a structure formed by several steel tubes welded together and separated with a membrane joint, as shown in Figure 1. The tube walls are mounted on the furnace of the boiler, which can simplify the structure and reduce its weight. During boiler operations, the heating surface of the tube wall is exposed to intense heat and chemical components (including furnace particles related to the combustion reaction). These lead to corrosion and wear, which permanently damage the tubes and affect the working life and performance of the tube walls [1–5]. When the corrosion and wear occur, the tube walls' thickness is affected, and there is a need to recover the lost thickness. The lost thickness recovery falls in three ways. The first is to take out the worn tube walls and replace them with new ones. Meanwhile, this leads to a boiler stoppage and affects its working time and

productivity. The second way is achieved by reducing the operating temperature of the steam, but this will affect the production efficiency of the plant [6]. The other way, which is the optimal solution, is to overlay the surface of the tube walls with a more corrosion-resistant alloy [7]. The overlay can be used on other parts such as pipes, vessels, valves, and tubes. It is utilized for repairing damaged parts to improve the reliability of the overlaid components [8]. Different overlay methods are employed to provide a protective layer such as thermal spraying, shielding manual arc welding, and gas metal welding. Each of these processes comes with some merits and shortfalls [9]. Nowadays, pulse gas metal arc welding (GMAW) is considered as the most commonly used technique in the industry to weld overlay a protection layer for the tube walls with different alloys such as ER309L stainless steel, Inconel 617 alloy [10], and Inconel 625 [11]. This is due to the easy automation, high productivity, flexibility (working for most welding positions and material), low heat input, and high deposition rate [12]. The alloy Inconel 625 is widely used as an overlay material for tube walls due to its corrosive resistant properties [13]. N. Kumar et al. [14] introduced some studies on nickel-based Inconel 625 hard overlays on AISI 316L plate by gas metal arc-welding-based hardfacing process. The weaving technique was adopted using robotic gas metal arc welding (GMAW) process to reduce the dilution percentage and contact angle.

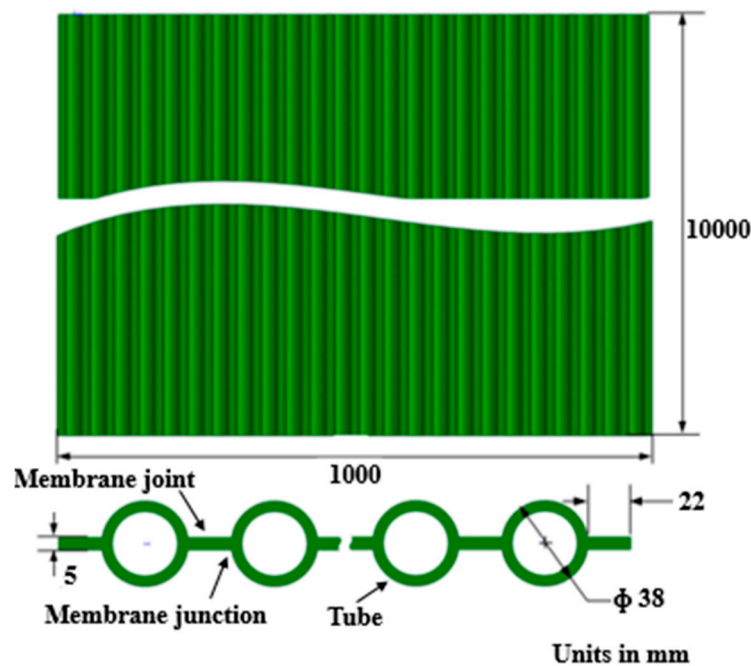


Figure 1. Schematic diagram of the boiler tube's wall.

Manual welding requires high labor strength and leads to low quality due to human error. The quality and productivity improved if the weld overlay process was executed automatically. Furthermore, the better features of the surface finish are achieved with the smallest dilution rate of the added material [15]. The automation of weld overlaying for huge dimensions and complex geometry of the tube walls constitute a major challenge, as shown in Figure 1. Recently, a few studies have been developed in the automatic welding field to solve such issues. Huilin Z et al. [16] developed an automatic welding system for a long-distance X-80 pipeline. The design included welding carrier, and the guide rail and self-shielded flux-cored wires technique. The equipment was designed without a tracking system. In another work, Li A et al. [17] designed an automatic welding machine based on programmable logic control (PLC). The design included a manipulator, positioner, and CO₂ gas welding techniques. This design is most suitable for a revolving workpiece. In a related study, Kim Y-B et al. [18] produced an automatic multilayer welding system for large containerships; the design included a touch sensor and welding sequence plan. The design is suitable for heavy metal

plates. While Dinham M et al. [19] implemented an automatic weld seam tracking with an optical system charged-coupled device (CCD camera) for steel pipe V groove, only suitable for plate butt joint. K. Xue et al. [20] proposed a robotic seam tracking system based on vision sensing and human-machine interaction for multipass metal active gas arc welding (MAG). In the design, the industrial camera was placed in front of the welding torch to monitor the welding area from the upper-left view, which distorts the welding images in the monitoring interface. Z. Fang et al. [21] introduced a vision-based robotic laser welding system for insulated mugs with fuzzy seam tracking control. During the welding process, a seam tracking system with fuzzy logic control method is presented to keep the torch precisely on the seam. J. Fan et al. [22] proposed a precise seam-tracking method for narrow butt seams based on a structured light vision sensor. The seam tracking includes a structured light vision sensor with optical filters, an extra LED light, laser stripe, and narrow butt. Besides, an image processing method for the vision sensor is designed to obtain welding torch deviations of narrow butt seams both in the horizontal and vertical directions.

Bug-o Systems [23] designed a portable automatic welding carriage with an adaptable welding manipulator. Three degrees of freedom (DOF) and pendular motion were implemented in this design. The carriage was fixed to the tube walls by two horizontal rails. The limitations of the study were the short stroke of the guide rails, which makes it difficult to overlay the membrane junction area between the tube surface and the membrane joint. The manipulator needs to reposition manually according to the desired beads. Furthermore, there is an absence of the weld path and the appropriate program for overlaying the tube walls of a known length. Dutra JC et al. [15] developed a computer numeric control (CNC) robot with four DOF to weld overlay the desired area of the tube walls via the GMAW technique using ER309L stainless steel. The limitations of the study are that the welding torch was perpendicular to the welded surface during the welding process. Furthermore, the absence of the weld-tracking system leads to the need to readjust the torch manually for the welding distortion and assembly error. Moreover, the robot was unsuitable for large workpieces and mass production. The movement of the welding carriage along the tube walls also can affect the surface finish of the tube walls.

Based on the literature review described above, there is no dedicated solution that has been proposed to weld overlay on both sections (membrane joint and tube surface). Therefore, the present research focuses on a dedicated design for the proposed automatic weld overlay system. To exploit the high welding speed and low deposition rates with less penetration, the vertical downward weld overlay approach via the pulse GMAW technique is used. Thus, a spray metal transfer with less spatters needs to be obtained. The system reduces the overlapping of each adjacent beads during the welding process by planning beads sequences. That is due to the large amplitudes oscillated by the welding torch. Thus, the sequence produces a better shape of beads. When the torch oscillates, three axes (X-motor, Y-motor, and rotation motor) move simultaneously. The distance between the nozzle end and the tube wall's surface is permanently unchanged. Moreover, the proposed system is flexible and programmable; it also allows the correction of welding trajectories.

The remainder of this paper is structured as follows: Section 2 presents a brief description of the mechanical system model adopted on our framework. Section 3 demonstrates the proposed methodology. Section 4 analyzes the mathematical model of automatic welding mechanisms. Section 5 explains the designed weld-tracking system. The control system design is presented in Section 6, while Section 7 presents the results and discussion. Finally, the main conclusions based on the obtained findings of our design and future work are described in Section 8.

2. Mechanical Design and Working Principle

The proposed mechanical structure of weld overlaying equipment includes the headframe, the gantry crane system, welding carriage, and contact-tracking sensor. To fit the requirements of the arc welding and the dimensions of the boiler tube walls, the model of the proposed automatic welding system design and analysis is performed using the three-dimensional software SolidWorks (Dassault

Systèmes, Vélizy-Villacoublay, France). The headframe structure was designed for the installation and vertical placement of the boiler tube walls to keep it stable during the welding process. The structure of the headframe was designed as a lattice component. It is supported by square tubes, which generally increase the rigidity of the structure. The tube walls were placed vertically on the tube holder, which was hoisted by cylinders, and installed on the headframe. The foundations filled with reinforced concrete are used to improve the stability of the head frame, as shown in Figure 2a.

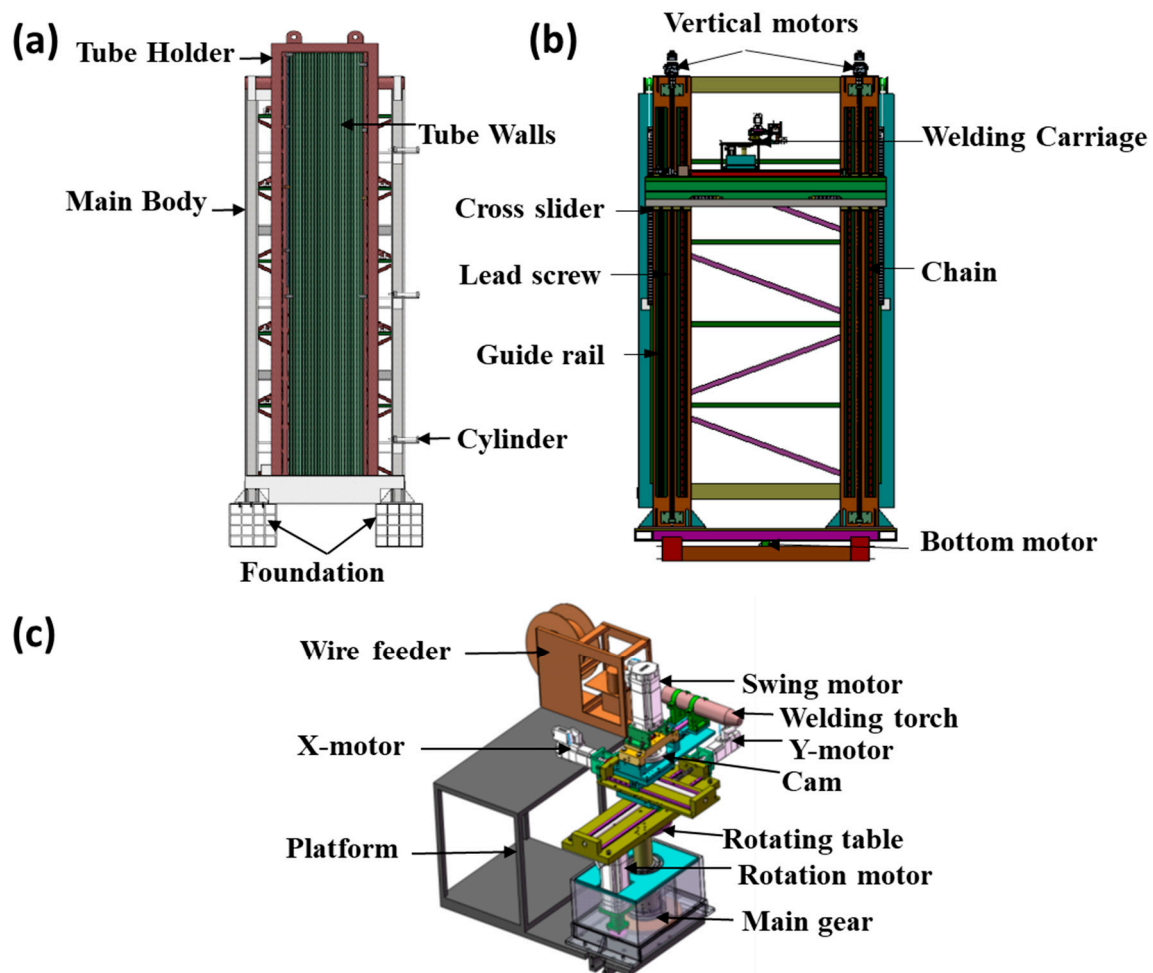


Figure 2. The mechanical structures and components of the proposed system. (a) Headframe; (b) gantry; (c) welding carriage.

The gantry lattice structures were designed for realizing the multi-axis movement of the welding carriage. The main components of the gantry part are the cross slider, guide rail, chain, platform, wire feeder mechanism, and the welding carriage. The welding carriage includes the torch posture, position, and oscillation mechanisms, which adjust the torch movement, as shown in Figure 2b. The gantry and its components are driven by motors to realize up and down, front and back, and left and right rotation of the welding torch. Eight motors are used in the gantry mechanism to realize an automatic weld overlay. Two vertical motors were placed at the top of the gantry. These synchronously drive the cross-slider and welding mechanism up and down.

The cross-slider motor drives the lead screw to move the welding carriage left and right. Therefore, the welding carriage is located near the surface of the overlaying workpiece. The whole gantry is driven forward and backward by the motor that is placed at the bottom gantry. The workpiece surface is composed of the plane and circular arc surface. During the welding process, the torch seems to be perpendicular to the welded surface (from the top view) and is rotated to adjust the posture by

rotation motor. The swing motor oscillates the welding torch. Finally, two adjustments motors are used to regulate the welding torch position relative to the boiler tube's wall in two axes, as depicted in Figure 2c.

The dimensions of the entire system are described as length \times width \times height. The headframe has dimensions of 3100 mm \times 3100 mm \times 10,425 mm. The gantry dimensions are 4040 mm \times 3500 mm \times 8070 mm, while the welding carriage has dimensions of 500 mm \times 933 mm \times 769 mm.

3. Weld Overlay Methodology

To realize the automatic weld overlaying and keep the proper overlapping between each two adjacent beads, it is necessary to plan the welding sequence. The geometry of the workpiece, the nozzle, overlapping between the adjacent beads, the angle between the wire, and the welded surface are the main influencing factors for automatic welding via pulse GMAW. The geometry of the boiler tube walls is considered as membrane joint, membrane junction, and tube surface. The required distance of one weld overlay cycle is 60 mm. The dimensions of the common nozzle are 20 mm in diameter and 75 mm in length. When the welding torch oscillates at the amplitude (swing width) of 8 mm, the nozzle will interfere with the tube walls. To overcome the interference, the dimensions of the nozzle were reduced to 14 mm in diameter and 100 mm in length. The proposed overlapping width of the beads located in the membrane joint and membrane junction is 1.5 mm; similarly, it is 2 mm for the tube surface beads.

The proposed beads distributed on the geometry of the tube walls were planned as one bead for the membrane joint (10), two beads for the membrane junctions (11, 12), and nine beads for the tube surfaces (1–9). The welding sequence is planned as (1–4), (5–8), 9, 10, (11–12), as illustrated in Figure 3. The distance between the wire end and the workpiece is 10 mm, and the angle between the welding wire and the membrane joint is 67.38 degree in the 11 beads. To make the welding torch oscillate smoothly, the wire does not pass through the center of the tube. The intersection point between the torch axis and membrane joint plane is 11.47 mm away from the tube center. Besides, the angle between the welding torch and membrane joint plane is 44.47 degree in the first bead. The beads 1 and 5 are symmetrical, with the same welding requirements.

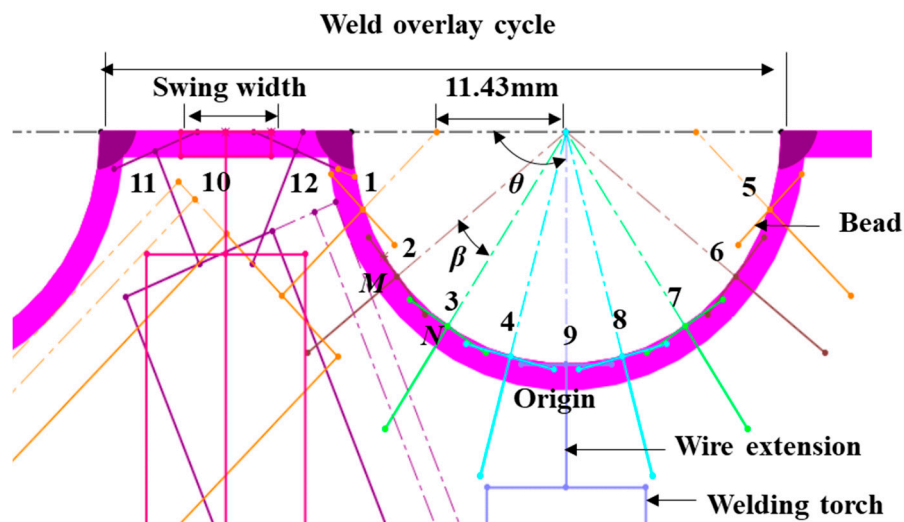


Figure 3. Schematic of weld beads sequence.

For beads 2, 3, 4, 6, 7, 8, and 9, it is not necessary to consider the interference between the nozzle and the overlays. The welding torch axis passes through the circular center of the tube. Table 1 shows the angles between the beads and the membrane joint. The angle β represents the rotation angle of the welding torch between two-weld beads, while θ is the angle between the welding torch and the membrane joint, as illustrated in Figure 3.

Table 1. The angles between the beads and membrane joint.

Bead No.	1,5	2,6	3,7	4,8	9,10	11,12
Angle (degree)	44.47	38.34	56.61	74.88	0	67.38

4. Mathematical Analysis of the Automatic Welding Mechanisms

The welding carriage includes weld tracking, posture change mechanisms. These components are physically connected and run according to the weld trajectory to achieve the weld overlay throughout the tube walls. According to the weld overlaying requirements, the strokes of x- and y-axes are analyzed and calculated. The coordinates and transformations of the welding torch were computed using the inverse kinematic theory [24].

When the welding torch posture and position are adjusted, the cross slider is stationary. Thus, a rectangular coordinate system was built on the cross slider. The coordinate system $\{O_1\}$ is established with the centerline of the cross-slider lead screw in the horizontal plane. Y_1 indicates the movement direction of the welding carriage, and X_1 represents the direction from the gantry to the head frame. The lead screw center at the left limit of the cross-slider acts as the origin of coordinates $\{O_1\}$. Z_1 is the vertical axis through the origin and is consistent with the right-hand rule, as shown in Figure 4. The center of the main gear is established as the coordinate system $\{O_2\}$. The directions of the coordinate $\{O_2\}$ is parallel to the $\{O_1\}$ due to the reason that the center of the rotating table $\{O_2\}$ is z_{12} away from the center of the cross slider $\{O_1\}$ in the Z direction.

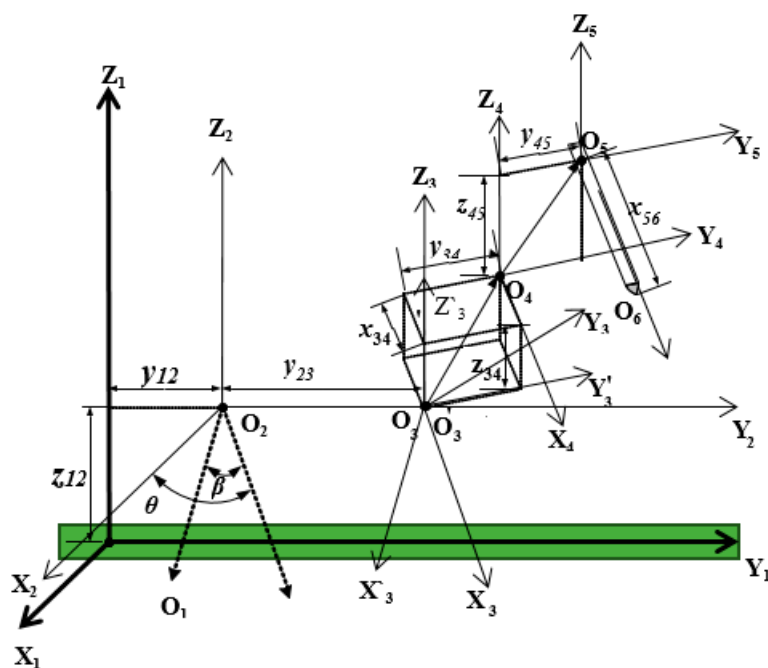


Figure 4. The coordinate systems of the cross slider and welding carriage.

The distance between Z_1 and Z_2 is y_{12} , which is the same as the distance with $\{O_1\}$ and the center of the main gear in the direction of Y_1 . During the weld overlaying process, the welding carriage moves along the cross-slider axis from left to right in the full cycle with y_{23} . Thus, the main gear center acts as the origin of the coordinate system $\{O_3\}$. X_3 and Y_3 in the coordinate system $\{O_3\}$ were considered as the X_2 and Y_2 rotating around the Z_2 axis by angle θ . The translation distance along the Y_2 axis is y_{23} . The coordinate system $\{O_4\}$ is established as the intersection of the cam center and the X motor shaft axes. X_4 represents the X-motor axis; y_4 is parallel to the Y motor axis. In contrast, the Z_4 direction follows the right-hand rule. The distances between $\{O_4\}$ and $\{O_3\}$ origins in X_3 , Y_3 , and Z_3 direction are x_{34} , y_{34} , and z_{34} , respectively. The x_{34} and y_{34} are the displacement of $\{O_4\}$ origin

in the X_3 and Y_3 directions when the welding torch moved from the original position to the M bead, as depicted in Figure 4. Z_{34} is the distance between the X motor axis and the main gear. At the origin, $\{O_4\}$ coordinate values in $\{O_3\}$ are $(0, 0, 183)^T$.

Thereafter, the intersection point of the welding torch center and Y_4Z_4 plane creates the coordinate system $\{O_5\}$. X_5 indicates the centerline of the welding torch; the Y_5 axis is parallel to axis Y_4 . During the movement of the welding carriage, the X_5 axis in the coordinate $\{O_5\}$ is parallel to the X-motor shaft axis.

The origin values of $\{O_5\}$ are $(0, y_{45}, z_{45})^T$ in $\{O_4\}$. The y_{45} and z_{45} are the fixed distances between $\{O_4\}$ and $\{O_5\}$ in Y_4 and Z_4 directions, respectively. The fixed distance between the welding torch end $\{O_6\}$ and $\{O_5\}$ in the X_5 direction is X_{56} . Table 2 shows the relative position parameters of the origin of each coordinate system.

Table 2. The relative position parameters of the origin of each coordinate system (mm).

Parameter	y_{12}	z_{12}	z_{34}	y_{45}	z_{45}	x_{56}
Value(mm)	385.00	185.0	183.0	209.7	170.0	338.5

Considering that, the original position of the welding torch is located in bead number 9. The torch moves from position 1 to position 12 in turn according to the beads sequence trajectory. The displacement of the torch end $\{O_6\}$ is $\Delta X_1, \Delta Y_1$ in the direction of X_1, Y_1 with respect to the coordinate system $\{O_1\}$; Table 3 shows the data values of the angle $\beta, \theta, \Delta X_1$, and ΔY_1 . When the welding torch is adjusted from the former bead M to the next bead N, as shown in Figure 4, the coordinate value of the welding torch end $\{O_6\}$ in $\{O_1\}$ is expressed by Equations (1) and (2). The X and Y motors drive the welding torch to move with displacements $x_{34'}$ and $y_{34'}$. Equations (3) and (4) are obtained from Equations (1) and (2).

$$\Delta^{O_1}P = \begin{pmatrix} [c(\theta + \beta) - c\theta](x_{34} + x_{56}) + \\ c(\theta + \beta)x'_{34} - s(\theta + \beta)y'_{34} - \\ [s(\theta + \beta) - s\theta](y_{34} + y_{45}) \\ \\ [s(\theta + \beta) - s\theta](x_{34} + x_{56}) + \\ s(\theta + \beta)x'_{34} + c(\theta + \beta)y'_{34} + \\ [c(\theta + \beta) - c\theta](y_{34} + y_{45}) \\ \\ 0 \end{pmatrix} \tag{1}$$

Table 3. The position change table of the welding torch end $\{O_6\}$ in $\{O_1\}$.

Bead	ΔX_1 (mm)	ΔY_1 (mm)	θ (Degree)	β (Degree)
origin→1	15.67	25.05	0	-45.53
1→2	-4.66	-2.31	-45.53	-6.13
2→3	-6.22	-6.79	-51.66	18.27
3→4	-3.78	-8.40	-33.39	18.27
4→5	14.66	-32.62	-15.12	60.65
5→6	-4.66	2.31	45.53	6.13
6→7	-6.22	6.79	51.66	-18.27
7→8	-3.78	8.40	33.39	-18.27
8→9	-1.00	7.56	15.12	-15.12
9→10	19.00	30.00	0	0
10→11	-0.77	2.34	0	22.62
11→12	0	-4.69	22.62	-45.24
12→origin	-18.23	-27.66	-22.62	22.62

Hint:

$$\begin{aligned}
 c\theta &= \cos \theta, s\theta = \sin \theta \\
 c(\theta + \beta) &= \cos(\theta + \beta), s(\theta + \beta) = \sin(\theta + \beta) \\
 \Delta^{O1}P &= \begin{pmatrix} \Delta^1P_x \\ \Delta^1P_y \\ \Delta^1P_z \end{pmatrix} = \begin{pmatrix} \Delta X_1 \\ \Delta Y_1 \\ 0 \end{pmatrix}
 \end{aligned} \tag{2}$$

The related data in Tables 1 and 2 are substituted into Equations (3) and (4), and the adjusted data of X, Y motors are obtained, as shown in Table 4. Thus, the displacement ranges that X and Y motor move through the lead screw in X and Y directions are -304.02 to 83.89 mm and -367.88 to 208.62 mm, respectively.

$$x_{34}' = c(\theta + \beta)\Delta X_1 + s(\theta + \beta)\Delta Y_1 - (1 - c\beta)(x_{34} + x_{56}) + s\beta(y_{34} + y_{45}) \tag{3}$$

$$y_{34}' = c(\theta + \beta)\Delta Y_1 - s(\theta + \beta)\Delta X_1 - s\beta(x_{34} + x_{56}) - (1 - c\beta)(y_{34} + y_{45}) \tag{4}$$

Table 4. The adjusted data of X, Y, and rotating motors.

Weld Bead	x34'(m)	y34'(mm)	Angle β (Degree)	X Displacement (mm)	Y Displacement (mm)
Origin→1	-257.93	207.49	-45.53	-257.93	207.49
1→2	-46.09	1.13	-6.13	-304.02	208.62
2→3	127.95	-40.99	18.27	-176.07	167.63
3→4	108.65	-79.04	18.27	-67.42	88.59
4→5	108.79	-421.69	45.53	41.38	-333.11
5→6	-16.43	-34.77	6.13	24.95	-367.88
6→7	29.80	131.01	-18.27	54.76	-236.87
7→8	-12.77	133.75	-18.27	41.99	-103.13
8→9	-41.98	103.12	-15.12	0.01	-0.01
9→10	19.00	30.00	0	19.01	29.99
10→11	64.88	-153.49	22.62	83.89	-123.50
11→12	-184.39	270.09	-45.24	-100.49	146.59
12→origin	100.50	-146.61	22.62	0.01	-0.02

5. Weld-Tracking System

The weld-tracking system includes the sensor and control algorithm. The sensor detects the deformation of the tube walls. The sensed deformations are tracked by the control algorithm to keep the distance between the welding torch and the tube walls unchanged. The weld-tracking system details are discussed in the following sections.

5.1. Sensor Structure

Concerning the geometry of tube walls, the deviation of the welding torch and workpiece are certainly sensed. The beads trajectory is tracked to assure a fixed distance between the torch and tube walls. By collecting and processing the deformation data, the direction and size of the deviation of the tube walls were calculated. The motors make the corresponding response according to the sensed data and adjust the distance between the tube walls and the welding torch. Figure 5a shows the scheme design of the displacement sensor.

As Figure 5b shows, A, B, and C are the three detectors of the displacement sensor. The detectors touch the tube. The three detectors move through the center of the tube, OC is perpendicular to the membrane joint. OA and OB are symmetrical to OC. However, the angle between the OA and membrane joint is α . To prevent the interference between A or B and the adjacent tube, the angle α value is chosen to be 45 degree.

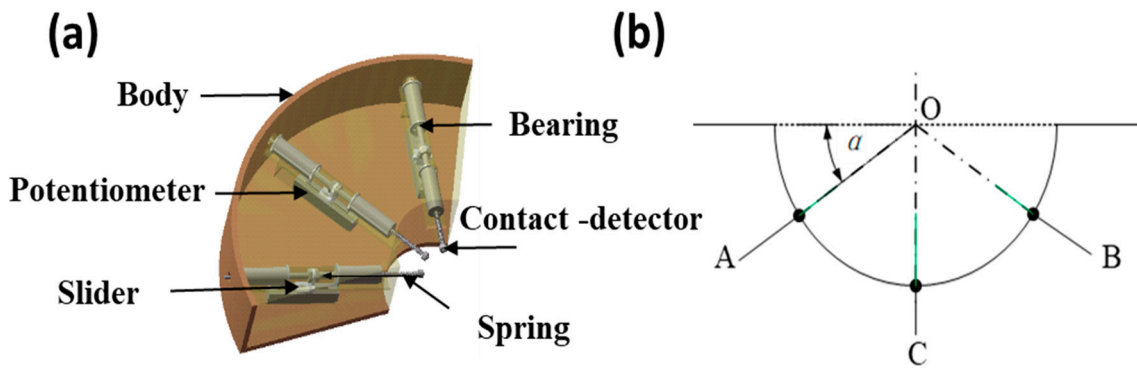


Figure 5. Sensor structure. (a) The scheme design of the displacement sensor; (b) the position sketch of the sensor through the center.

5.2. Working Principle of the Sensor

The equivalent circuit of the sensor is illustrated in Figure 6. When the tube offset value changes, the tracking mechanism regulates the distance between the welding torch and the tube. Therefore, the welding torch keeps track of the tube with the correct welding location. The sensor is made up of slider potentiometers linked to the sensor’s detector. The spring is used to keep the detector’s contact on the tube surface. When the detector of the sensor moves upward and downward along the tubes, the output voltages U_A , U_B and U_C across the potentiometers change.

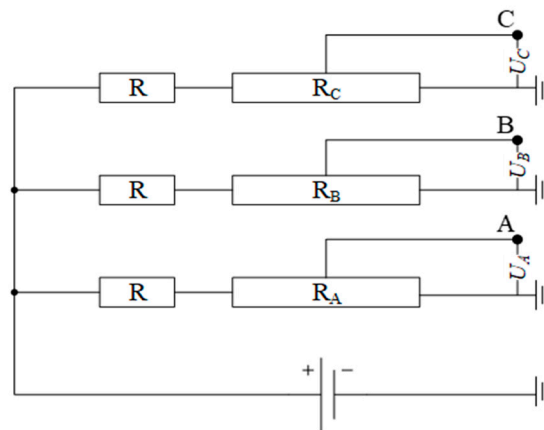


Figure 6. The equivalent circuit of the proposed sensor.

The voltage differences are then compared with a set threshold voltage. The differences are interpreted as deformations since the sign and magnitude of the voltage difference are proportional to the direction and value of the detector displacement. The association between the coordinate values (a , b) of the tube center after deformation and the displacements (ΔL_a , ΔL_b , ΔL_c) of the detectors (1, 2, and 3) can be developed by making computable analysis. For the starting points of the sensor, the center of the tube is set to be the origin of the coordinate system, the X-axis is parallel to the membrane wall, and the Y-axis is perpendicular to the tube walls. Therefore, depending on the dimensions of the tube, the detectors will come into contact with the tube at initial coordinates (A, C, B): $(-13.433, -13.433)$, $(0, -19)$, $(13.433, -13.433)$. Figure 7 illustrates the sensor schematic diagram with the initial contact position of the detectors.

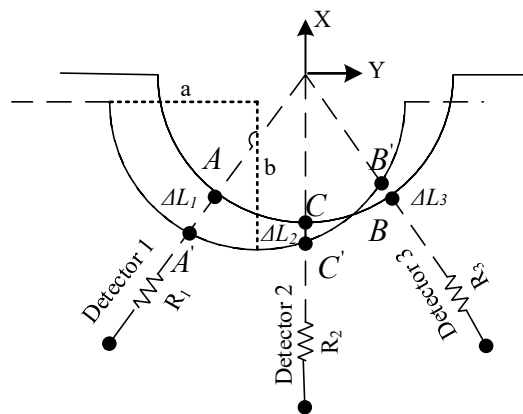


Figure 7. Schematic diagram of sensor.

5.3. The Tube Walls Deviation

The presence of deformations in the tube walls changes the relative position of the tube center. As can be seen in Figure 7, the tube position might be reformed from AB to $A'B'$ and the displacements of the detectors from their initial points will be ΔL_1 , ΔL_2 , and ΔL_3 accordingly. The displacements have positive and negative values, depending on the detector's moving direction, with or against the detector direction. The coordinates of the corresponding three contacts points after deformation (A' , C' , B') are as follows:

$$(-13.433 + \Delta L_1 \cos 45^\circ, -13.433 + \Delta L_1 \sin 45^\circ), (0, -19 + \Delta L_2), (13.433 - \Delta L_3 \cos 45^\circ, -13.433 + \Delta L_3 \sin 45^\circ)$$

Here $^\circ$ indicates degree; therefore, the following Equations can be developed as

$$(-19 \cos 45^\circ + \Delta L_1 \cos 45^\circ - a)^2 + (-19 \sin 45^\circ + \Delta L_1 \sin 45^\circ - b)^2 = 19^2 \quad (5)$$

$$a^2 + (-19 + \Delta L_2 - b)^2 = 19^2 \quad (6)$$

$$(-19 \cos 45^\circ + \Delta L_3 \cos 45^\circ - a)^2 + (-19 \sin 45^\circ + \Delta L_3 \sin 45^\circ - b)^2 = 19^2. \quad (7)$$

Equations (5)–(7) are the three contact points of the detectors after deviation in x- and y-direction. The variables a and b are the values of the tube center after the deformation with respect to x- and y-axes. The following results were obtained by solving these Equations:

$$a = \frac{[\Delta L_3^2 - \Delta L_2^2 - 38(\Delta L_3 - \Delta L_2)] \sqrt{2}(38 - (\Delta L_3 + \Delta L_1)) - \sqrt{2}(\Delta L_3 - \Delta L_1)[\Delta L_1^2 - \Delta L_3^2 - 38(\Delta L_1 - \Delta L_3)]}{[2(\Delta L_3 - 19)(\Delta L_3 - \Delta L_1) - (19\sqrt{2} - 38 + 2\Delta L_2 - 2\Delta L_3)] \sqrt{2}(38 - (\Delta L_1 + \Delta L_3))} \quad (8)$$

$$b = \frac{[\Delta L_3^2 - \Delta L_2^2 - 38(\Delta L_3 - \Delta L_2)][\sqrt{2}(38 - (\Delta L_3 + \Delta L_1)) - [\Delta L_1^2 - \Delta L_3^2 - 38(\Delta L_1 - \Delta L_3)] \sqrt{2}(\Delta L_3 - 19)]}{[2(\Delta L_3 - 19)(\Delta L_3 - \Delta L_1) - \sqrt{2}(38 - (\Delta L_3 + \Delta L_1))][19\sqrt{2} - 38 + 2\Delta L_2 - \sqrt{2}\Delta L_3]} \quad (9)$$

5.4. Control Algorithm (ANFIS)

The fuzzy logic is one of the most effective concepts in control engineering and is widely used in real-time control systems. Fuzzy logic coupled with neural networks yields substantial results. The resulting technique inherits the ability of neural networks in learning capability with fuzzy logic for knowledge representation to create a new technique well known as neuro-fuzzy networks. This hybrid technique enhances the controller's reliability and performance in terms of cost [25,26]. The proposed close loop of the control system combines three parts—namely, adaptive neuro-fuzzy inference system (ANFIS) as the controller, the sensor in the feedback, and the motor driver connected to the output of the ANFIS controller. In the ANFIS design, the neural network is matched with a suitable rule base logic, which is realized using backpropagation (BP). The signals come from the sensor according to the real status of the deformed place in the tube walls; these signals are then compared with the threshold

value according to the welding accuracy. The input error signals (a) and (b), and x and y displacements are the output for the ANFIS controller. Figure 8 shows the close loop control for the proposed system.

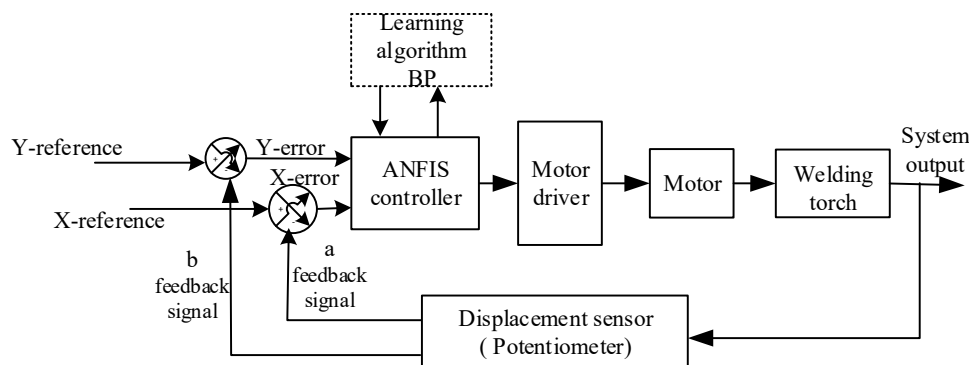


Figure 8. The proposed closed control system. BP—backpropagation.

6. Control System Design

The driving and control systems need to be configured to realize the multi-axis movement of the welding torch via AC drivers. The SIMOTION controller (CU320-2DP and D435-2DP/PN, Munich, Germany), which is made by Siemens Ltd., was selected to control the multi-axis movement of the motors. To prevent the interference of the welding torch with the tube walls, the X, Y, and rotation motor can be moved by interpolation. The two vertical motors placed on top of the gantry should be moved synchronically to prevent the inclination of the cross slider. The cross slider, swing, and gantry bottom motors are controlled separately. The load on the controller is eased by using a dual-controller architecture. The human-machine interface (HMI) is used as the interface to control the welding parameters and greatly improve its practicality. The position, orientation, and sequence of the beads are calculated and then sent to the controller. The controller plans the required trajectory then guides the welding torch. The controller communicates with the welding power via industrial Ethernet to achieve real-time control of the welding power parameters. Figure 9 shows the structure of the control system. During the weld overlay process, five motors were realized. When the two vertical motors run, the welding carriage moves from the up to down position at the appropriate welding speed. The swing motor makes the torch oscillate at the required frequency according to the required bead width. The ANFIS algorithm, according to the data acquired from the sensor, would adjust X and Y motors as the tracking axes. After finishing the weld overlay over the whole tube walls, the bottom motor should run to move the gantry back with a suitable space, so a new workpiece is then installed.

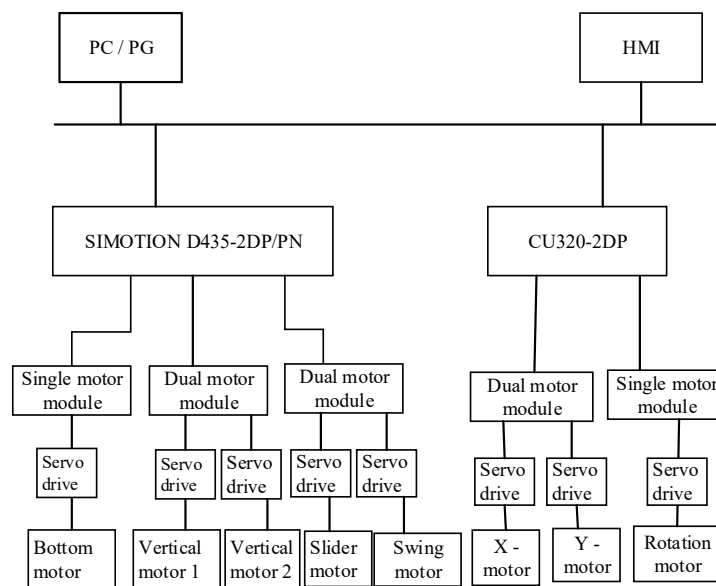


Figure 9. Control system flow chart. HMI—human–machine interface.

7. Results and Discussion

To verify the validity of the proposed system's aforementioned kinematics and methodology, several tube walls with dissimilar height were overlaid in the workshop, as shown in Figure 1. The vertical downward automatic weld overlay was applied for the tube walls via pulse GMAW technique. An Inconel 625 alloy wire of diameter 1.2 mm was used. The shielding gas is 99.9% Argon. The welding torch was inclined upward, and the included angle of the welding torch axis with the vertically downward direction is about 75–80 degrees. The arc force always blows the droplet to the molten pool. A spray metal transfer with less spatters was obtained.

In the vertical downward welding position, as the deposited material is liquid, the arc acts on the molten pool surface and the lowest penetration can be obtained in comparison with other welding positions (such as downhead welding, horizontal position welding, etc.), the low dilution rate will be achieved. The molten pool is acted by gravity, surface tension, and arc force, which is significantly influenced by the geometry of the weld beads. The surface tension of the molten pool has a reverse relationship with the temperature. Once the welding current is high, the temperature of the molten pool is high and the surface tension is low. Consequently, the molten pool is easy to drop. At the same time, when the arc force—which is the plasma force—becomes large, the penetration and the dilution are increased. However, when the welding current is low, the molten pool will not drop, and small dilution can be obtained with low efficiency. Therefore, when the welding speed is high, the forward and backward welds will not be smoothly continuous, there will also be a gap between the two adjacent welds. However, once the welding speed is low, there will be much overlap between the two welds, and there will be much heat, which distorts the workpiece.

Moreover, the welding torch oscillates to form an enlarged uniform bead. Once the oscillation frequency is high, the weld unit length receives less heat energy and the penetration is low. Consequently, the good fusion cannot be achieved; while, when the oscillation frequency is low, the weld unit length receives much heat energy, so the molten pool will drop and the dilution is high.

The range of the welding parameters used in the experiment is as follows: welding current is in the range of 120–160 A, welding voltage is in the range of 22–25 V, welding frequency is between 10–12 Hz, and the welding speed is around 0.6–0.8 m/min. The pulsed GMAW process was applied at the aforementioned parameters to provide a better arc welding stability. The weld overlay of the vertical tube walls followed the sequence of carrying out the weld beads, starting from the tube, then directly heading to the membrane joint, and finally, on the membrane junction.

Thus, all beads have a width of 8–10 mm and an overlay layer thickness measured in the range of 2–2.2 mm, which saves lots of expensive overlay material. The overlapping width of the membrane joint and membrane junction beads is 1.5 mm; likewise, it is 2 mm for the tube beads, which can fit the proposed beads analyses. To calculate the quality of the weld overlay, the penetration is measured in the range of 0.1–0.6 mm, and the dilution is calculated in the range of 2–4%. The surface of the weld overlay structure has a good finish. The weld overlay results on the tube walls, as depicted in Figure 10, properly fit the weld overlay requirements for the boiler tube walls.

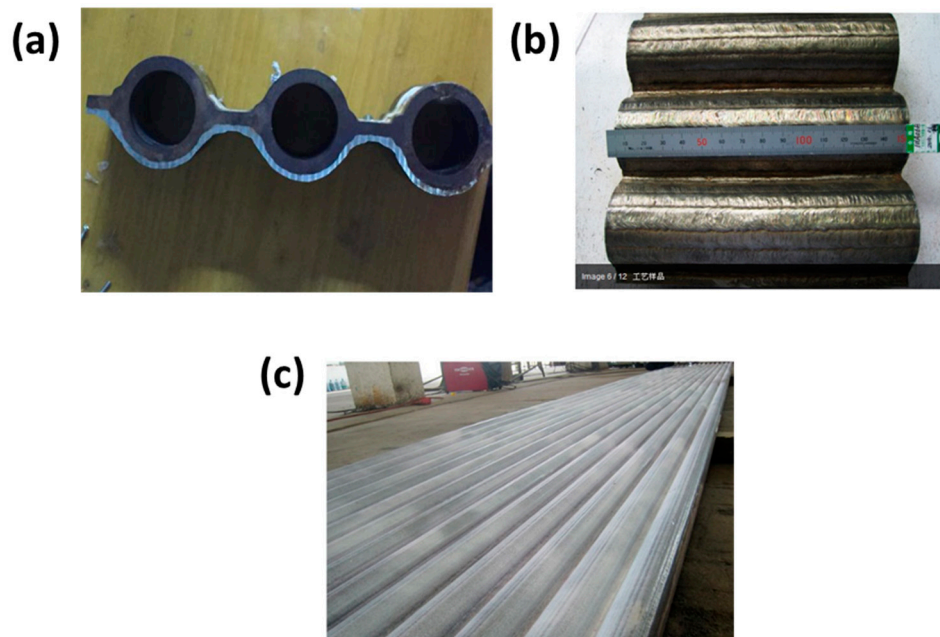


Figure 10. (a) The tube walls section; (b) weld overlay result on the tube panels; (c) the entire tube wall's surface.

Table 5 shows a comparison between our proposed design and previous related designs. Our design offers a much-improved functionality. It can be seen that the proposed design achieves a higher welding speed in the range of 36 m/s to 48 m/s, frequency ranging between 10 Hz and 12 Hz, and dilution rate in the range of 2% to 4%. However, the Dutra design achieves a lower welding speed ranging from 21 m/s to 25.2 m/s, frequency up to 3.8 Hz, and dilution rate up to 28%. Based on the obtained results, it is noted that the proposed design outperforms the Dutra design in terms of welding speed, frequency, and dilution rate. This is attributed to the fact that the welding torch in our design is horizontally perpendicular to the welding surface, with a rotation degree of up to 80 degree. Besides, we exploited the weld-tracking system to control the welding distortion and assembly error using the ANFIS algorithm, and the DOF adapted by our design is 6. However, in Dutra design, the welding torch is vertically perpendicular to the welding surface. This, in turn, limits the welding speed and frequency, and increases the dilution rate. In addition, the DOF used by Dutra is 4.

Similarly, the main results have been compared with the study by P. Kumar et al. [14]. Based on Table 5, it can be seen that the P. Kumar design achieves a welding speed up to 15 m/s, frequency up to 2 Hz, welding current up to 120 A, and dilution up to 25.51%. It should be noted that Figure 11 shows the average of the parameters illustrated in Table 5.

Moreover, our design is more advantageous due to the fact that it is suitable for mass production, while Dutra is limited to small workpieces. Besides, we exploited the weld-tracking system to control the welding distortion and assembly error using the ANFIS control algorithm. Furthermore, the proposed design improves the degree of automation and increases the productivity significantly. Consequently, the system provides advantages such as reducing labor costs and improving the quality

of the welded surface finish, achieving a better arc welding stability and reducing the dilution, which saves lots of expensive overlay material. Finally, this research provides further development for the automatic welding systems than others.

Table 5. A comparison of the proposed design with some previously published work.

Ref.	Welding Process	Geometry	Parameters				Material
			Welding Speed (m/s)	Frequency (Hz)	Welding Current (A)	Dilution %	
The proposed design	pulse GMAW	Boiler tube walls	36–48	10–12	130–140	2–4	Inconel 625
J. Dutra et al. [15]	pulse GMAW	Boiler tube walls	21–25.2	3.8	127	28	ER309L stainless steel
N. Kumar et al. [14]	GMAW	Thick plate	15	2	120	25.51	Inconel 625

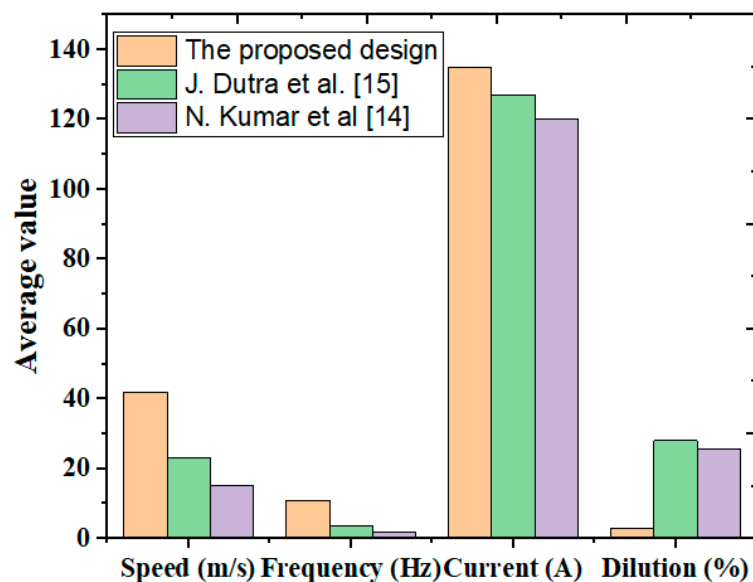


Figure 11. The comparison between the proposed design and previously published designs.

8. Conclusions

A dedicated automatic weld overlay system is presented to provide an effective protection layer to reduce the corrosion and wear of the boiler tube walls. The proposed design is comprised of the headframe, gantry, and welding carriage. The vertical downward weld overlay was applied via the pulse GMAW technique. Some conclusions are drawn as follows:

- A weld overlay methodology is developed based on the geometry of the tube walls, the number and sequence of the beads were planned. The SIMOTION controller was employed to control the welding torch movement according to the weld overlay method and to run the two vertical motors synchronously, while the X, Y, and rotation motors run by interpolation.
- A weld-tracking system that consists of a contact displacement sensor based on the potentiometer principle and the ANFIS controller based on the BP algorithm solve the problem of weld distortions, assembly errors, and the deformation of the tube walls, and correct the offset between the welding torch and workpiece.
- The experiment results show that the proposed design properly fits the boiler tube wall's weld overlay requirements with low dilution in the range of 2–4%, and with good surface finish. Furthermore, it improves the degree of automation and increases productivity significantly.

Consequently, the system provides advantages such as reducing labor costs and improving the quality of the welded surface.

- For future work, we plan to employ the Kalman filter and the laser vision system in designing the automatic weld-tracking system.

Author Contributions: Conceptualization, T.S., and A.S.; methodology, A.S., and T.S.; software, T.S., A.S., and G.P.; validation, G.P., A.S., and T.S.; formal analysis, A.S., and T.S.; experimental execution T.S. and A.S.; investigation, I.D., and A.S.; resources, A.S., and I.D.; data curation, A.S.; writing—original draft preparation, A.S.; writing—review and editing, A.S., T.S., and B.S.; visualization, A.S., I.D., and G.P.; supervision, T.S. and B.S.; project administration, T.S. and A.S.; funding acquisition, T.S.; A.S. and T.S. contributed equally to this work. All authors have read and agreed to the published version of the manuscript.

Funding: This research received no external funding.

Acknowledgments: The authors thank the Suzhou Hailu Heavy Industry CO., LTD., for their technical support. Moreover, the authors deeply thank Waleed M. Ismael, Sharaf Saifan, Alaa thobhani, Younis Ibrahim, Zaid Yemeni, Ebraheem Al-Qadasi, Hisham Manea, Gallab Al Badani, Taqi Aden, and Hamza Almadani for the valuable comments, suggestions, dedication, and commitment to the development of this work.

Conflicts of Interest: The authors declare no conflict of interest.

References

1. Alipour, Y.; Henderson, P.; Szakálos, P. The effect of a nickel alloy coating on the corrosion of furnace wall tubes in a waste wood fired power plant. *Mater. Corros.* **2014**, *65*, 217–225. [[CrossRef](#)]
2. Talus, A.; Alipour, Y.; Norling, R.; Henderson, P. Effect of sewage sludge addition on initial corrosion of 16Mo3 and 310S when exposed in a used wood fired boiler. *Mater. Corros.* **2016**, *67*, 683–692. [[CrossRef](#)]
3. Wang, B.Q. Erosion-corrosion of coatings by biomass-fired boiler fly ash. *Wear* **1995**, *188*, 40–48. [[CrossRef](#)]
4. Collins, J.A. A practising engineer's experiences in overcoming inherent design problems in thermal power station boilers. *Int. J. Pres. Ves. Pip.* **1995**, *61*, 157–175. [[CrossRef](#)]
5. Alipour, Y.; Viklund, P.; Henderson, P. The analysis of furnace wall deposits in a low-NO_x waste wood-fired bubbling fluidised bed boiler. *VGB Power Tech.* **2012**, *92*, 96–100.
6. Bankiewicz, D. Corrosion Behaviour of Boiler Tube Materials during Combustion of Fuels Containing Zn and Pb. Ph.D. Thesis, Abo Akademi University, Turku, Finland, 2012.
7. Alipour, Y.; Henderson, P. Corrosion of furnace wall materials in waste-wood fired power plant. *Corros. Eng. Sci. Techn.* **2015**, *50*, 355–363. [[CrossRef](#)]
8. Gupta, S.K.; Mehrotra, S.; Raja, A.R.; Vashista, M.; Yusufzai, M.Z.K. Effect of welding speed on weld bead geometry and percentage dilution in gas metal arc welding of SS409L. *Mater. Today Proc.* **2019**, *18*, 5032–5039. [[CrossRef](#)]
9. Nouri, M.; Abdollah-Zadeh, A.; Malek, F. Effect of welding parameters on dilution and weld bead geometry in cladding. *J. Mater. Sci. Technol.* **2007**, *23*, 817–822.
10. Adamiec, J.; Konieczna, N. The welded joints structure of the Inconel 617 alloy designed for high temperature operation in supercritical parameters boilers. *Arch. Met. Mater.* **2020**, *65*, 243–255.
11. Kannan, T.; Yoganandh, J. Effect of process parameters on clad bead geometry and its shape relationships of stainless steel claddings deposited by GMAW. *Int. J. Adv. Manuf. Technol.* **2010**, *47*, 1083–1095. [[CrossRef](#)]
12. Praveen, P.; Yarlagadda, P.K.; Kang, M. Advancements in pulse gas metal arc welding. *J. Mater. Process. Technol.* **2005**, *164*, 1113–1119. [[CrossRef](#)]
13. Alvarães, C.P.; Madalena, F.C.A.; De Souza, L.F.G.; Jorge, J.C.F.; Araújo, L.S.; Mendes, M.C. Performance of the INCONEL 625 alloy weld overlay obtained by FCAW process. *Rev. Mater.* **2019**, *24*, 1–12. [[CrossRef](#)]
14. Kumar, N.P.; Shanmugam, N.S. Some studies on nickel based Inconel 625 hard overlays on AISI 316L plate by gas metal arc welding based hardfacing process. *Wear* **2020**. [[CrossRef](#)]
15. Dutra, J.C.; Bonacorso, N.G.; Silva, R.H.G.E.; Carvalho, R.S.; Silva, F.C. Development of a flexible robotic welding system for weld overlay cladding of thermo electrical plants' boiler tube walls. *Mechatronics* **2014**, *24*, 416–425. [[CrossRef](#)]
16. Huilin, Z.; Changjiang, W.; Xuemei, Y.; Xinsheng, W.; Ran, L. Automatic welding technologies for long-distance pipelines by use of all-position self-shielded flux cored wires. *Ng. B* **2014**, *1*, 113–118. [[CrossRef](#)]

17. Li, A.; Zhang, C.H.; Li, H.L.; Xu, Z.Y.; Chen, X.H.; Qin, G.L.; Ye, S.W. Design of automatic welding machine based on PLC. In Proceedings of the 4th International Conference on Intelligent Computation Technology and Automation, Washington, DC, USA, 28–29 March 2011; pp. 627–630.
18. Kim, Y.-B.; Kim, J.-G.; Jang, W.-T.; Park, J.-R.; Moon, H.-S.; Kim, J.O. Development of Automatic Welding System for Multi-Layer and Multi-Pass Welding. In Proceedings of the 17th World Congress, the International Federation of Automatic Control, Seoul, Korea, 6–11 July 2008; volume 41, pp. 4290–4291.
19. Dinham, M.; Fang, G. Autonomous weld seam identification and localisation using eye-in-hand stereo vision for robotic arc welding Robot. *Comput. Integr. Manuf.* **2013**, *29*, 288–301. [[CrossRef](#)]
20. Xue, K.; Wang, Z.; Shen, J.; Hu, S.; Zhen, Y.; Liu, J.; Wu, D.; Yang, H. Robotic seam tracking system based on vision sensing and human-machine interaction for multi-pass MAG welding. *J. Manuf. Process.* **2020**. [[CrossRef](#)]
21. Fang, Z.; Weng, W.; Wang, W.; Zhang, C.; Yang, G. A vision-based robotic laser welding system for insulated mugs with fuzzy seam tracking control. *Symmetry* **2019**, *11*, 1385. [[CrossRef](#)]
22. Fan, J.; Jing, F.; Yang, L.; Long, T.; Tan, M. A precise seam tracking method for narrow butt seams based on structured light vision sensor. *Opt. Laser. Technol.* **2019**, *109*, 616–626. [[CrossRef](#)]
23. All Position Overlay System. Available online: https://www.bug.com/wpcontent/uploads/bsk-pdf-manager/2019/09/Overlay_Bro-3-19.pdf (accessed on 9 August 2020).
24. Liu, B.L.; Zhang, F.; Qu, X.; Shi, X. A rapid coordinate transformation method applied in industrial robot calibration based on characteristic line coincidence. *Sensors* **2016**, *16*, 239. [[CrossRef](#)] [[PubMed](#)]
25. Rashidi, F. Sensorless speed control of induction motor derives using a robust and adaptive neuro-fuzzy based intelligent controller. In Proceedings of the 2004 IEEE International Conference on Industrial Technology, Los Alamitos, CA, USA, 8 December 2004; pp. 617–627.
26. Aware, M.V.; Kothari, A.G.; Choube, S.O. Application of adaptive neuro-fuzzy controller (ANFIS) for voltage source inverter fed induction motor drive. In Proceedings of the 3rd International Power electronics and Motion Control Conference, Beijing, China, 15–18 August 2000.



© 2020 by the authors. Licensee MDPI, Basel, Switzerland. This article is an open access article distributed under the terms and conditions of the Creative Commons Attribution (CC BY) license (<http://creativecommons.org/licenses/by/4.0/>).